RUSSIAN CHEMICAL REVIEWS
Uspekhi Khimii

May 1971

U.D.C. 661.66,661.97/.99

Vitreous Carbon (Preparation, Properties, and Applications)

V.D.Chekanova and A.S.Fialkov

Vitreous carbon, one of the most important materials based on graphite carbon, is outstanding in its high mechanical strength, resistance towards aggressive media, and imperviousness to gases. Because of these unique properties, there has been a rapid growth in the range of articles made of vitreous carbon and in the number of applications.
The methods of production, formation mechanism, structure, properties, and the range of applications of vitreous carbon are described in this review. 97 references.

CONTENTS

I. Introduction 413
II. Production of vitreous carbon and fabrication of vitreous carbon articles 413
III. Properties of vitreous carbon 419
IV. Applications of vitreous carbon 427

I. INTRODUCTION

Modern technology has created a requirement for new constructional materials able to withstand high temperatures and aggressive media. One such material is artificial graphite. This material, however, though inert towards many reactive media, cannot be used at the boundary between two media because of its high permeability (due to the presence of a developed structure of pores and channels).

High-strength materials which are impervious to gases and liquids are urgently needed for a number of industrial applications. So far the need has been met by two materials: pyrolytic graphite[1] and vitreous carbon. These materials differ very substantially in their methods of preparation and in their properties: whereas pyrolytic graphite shows a marked anisotropy of thermal, electrical, and mechanical properties, vitreous carbon shows no anisotropy at all.

This review deals with the methods of preparation, the properties, and the fields of application of vitreous carbon.

Vitreous carbon is a new material, with a number of specific properties not found in the previously known modifications of carbon[2-4].

The study of vitreous carbon offers both practical and scientific interest, because this material is one of the non-graphitising forms of carbon, about which little is known.

II. PRODUCTION OF VITREOUS CARBON AND FABRICATION OF VITREOUS CARBON ARTICLES

Vitreous carbon and vitreous carbon articles can be produced by the thermal decomposition of some carbonaceous materials which give carbonised pyrolysis products without forming an intermediate liquid phase[5].

The first disclosure[6,7] of the production of an impervious form of carbon, using cellulose as the starting material, appeared in 1957. The process involved the following operations: preparation of an aqueous suspension in which the fibrous structure of cellulose is destroyed, precipitation of the product from suspension, and carbonisation with exclusion of air, followed by graphitisation[8-11]. Wheat-chaff cellulose, purified from lignin or xylan[6,12-15], may be used as the raw material for the production of impervious carbon.

Shortly after the first report of the preparation of this material, American, Japanese, French, and other papers discussed its properties and technical-scale production[6-17]. The raw material in this case can be synthetic resin of the resol (A-stage resin) or novolac (soluble phenol–formaldehyde) type[18,19], furfuryl alcohol or furfural[20-22], or polynuclear aromatic hydrocarbons[23,24]. The resins are carbonised with or without a catalyst by slow heating in a reducing or a neutral atmosphere[18,25,26].

Vitreous carbon can be prepared also from previously carbonised cellulose and synthetic resin, taken in the ratio of 3 : 7 by weight[27].

Some work has been done on the effect of filler additives to the cellulose dispersion[12]: the product was shown to remain impervious to gases even after the addition of fillers such as carbon black and colloidal graphite. The effect of the filler is largely dependent on the porosity and particle size of the filler itself. Thus, petroleum coke is too porous to be used as a filler for articles impervious to gases.

The addition of fillers can be a desirable step, since they do not degrade the high-temperature properties of the final product. Fillers lead to shorter production cycles, since they reduce the amount of material to be decomposed and the volume of volatile products evolved during the reaction.

A method[28] of production of vitreous carbon from furfuryl alcohol and furfural employs fillers of the same compounds, after hardening and crushing. This method evolves fewer volatile products, and the shrinkage of the manufactured articles is correspondingly reduced. The process is also cheaper, because hardening residues can be utilised.

Yamada and Takata[29] have proposed a method in which furfuryl alcohol or its initial condensation products are deposited in successive layers on the surface of a former, with or without the addition of carbon powder or chopped fibre. The resulting product is then graphitised or carbonised in the normal way. The advantage of this method is that volatile products are evolved more uniformly from the surface of the formed article during the hardening stage, and the quality of the product is thereby improved.

A preliminary degassing treatment of the components in vacuo is said[30] to improve the mechanical properties of the product, since it reduces the yield of volatiles during carbonisation.

Pyrolysis conditions (and in particular the rate at which the polymers are heated to the maximum temperature, and the time for which they are held at this temperature) can have a profound effect on the direction and the extent of the thermochemical reactions, and on the quality of the resulting non-porous material.

The technological production cycle of vitreous carbon occupies 2–4 months, the duration of the preliminary operations increasing in proportion to the maximum temperature which the vitreous carbon product is required to withstand[2].

Because of the extreme hardness of vitreous carbon, machining operations on the material are not straightforward, but they can be carried out with diamond-tipped tools, ultrasonic cutters, and grinding machines with carborundum wheels[2].

Most of the articles made of vitreous carbon do not require machining. The material is usually pressed to the finished size or cast into a mould[31] with allowance for shrinkage during heat treatment.

Tubular forms are made by the centrifugal forming method[32,33]. In one method of forming large cylindrical objects[34,35] the thermally reactive composition is cast into a former with a cylindrical core. Former and core are counter-rotated during hardening of the resin to avoid adhesion to the walls and to facilitate release of the article from the former.

Articles of many different shapes can be made of vitreous carbon: disks, tubes, cylinders, crucibles, beakers, boats, etc.[3] The maximum size of these articles which can be achieved in practice has been identified: in most cases the wall thickness is less than 3 mm. Tubes up to 1 m long and 40 mm in diameter have been made, as well as beakers of 3-litre capacity, disks up to 250 mm in diameter, and plates 100 × 500 mm. With especially close control over the composition of the resin, and the temperature and pressure during heat treatment, it is possible to make[25] rods 5–10 mm in diameter, articles with a wall thickness up to 6.3 mm, and crucibles up to 10 P in capacity.

In addition to articles of conventional shape, more unusual forms can be made of vitreous carbon: spheres 0.2–1.0 mm in diameter, tape weighing only a few mg per cm length, and vitreous carbon fibre[36-38]. The latter is made from furfuryl alcohol or furfural resin, which is hardened, drawn through a die under a pressure of 5 kg cm^{-2}, and carbonised in an inert atmosphere[39].

Vitreous carbon fibre has recently been prepared by extruding a mixture of resol, novolac, and furan resin (7 : 2 : 1 or 8 : 1 : 1 parts by weight), followed by rapid cooling, hardening, and carbonisation. Depending on the size of the orifice used for extruding the mixture, filaments 6–25 μm in diameter can be obtained[40].

The chemistry of vitreous carbon is the chemistry of the pyrolysis of synthetic resins. On heating a furfural–phenol–formaldehyde resin (FPFR), changes in weight and in composition are observed (Fig. 1 and Table 1)[41,42].

By monitoring the weight loss on heating, the thermal decomposition of the resin to the stage of carbonisation can be characterised. Heat treatment at 1200° gives an abundant evolution of pyrolysis products (low-molecular-weight gaseous species). The loss in weight under these conditions can be greater than 50%. On further carbonisation the weight change becomes insignificant and the weight curve runs parallel to the temperature axis.

The changes in chemical composition indicate a continuous succession of chemical reactions, the solid residue becoming gradually carbonised. On heating the resin at 1200°, the carbon content increases from 68.3 to 97.6% whilst the oxygen content decreases from 21.7 to 0.1%. The nitrogen and hydrogen contents decrease at the same time. However, the product which has been carbonised at 1200° still contains an appreciable amount of nitrogen (1.8%). Graphitisation gives an even purer carbonaceous material.

It has been found experimentally[41] that the insoluble fraction after heating FPFR to 100° amounts to 75%. On further heating the resin to 150°, the proportion of high-temperature compounds increases, and the insoluble frac-

tion becomes 95%. After treatment at a still higher temperature a completely insoluble polymer is obtained. The observed transition from a soluble to an insoluble polymer is evidence of chemical reactions within the material, confirmed by the change in free phenol and furfural contents during hardening of the resin. Thus, whereas a product containing 35% of free furfural and about 4% of free phenol is obtained after heating the material to 80°, no free components can be detected in the solid product after heat treatment at 200°.

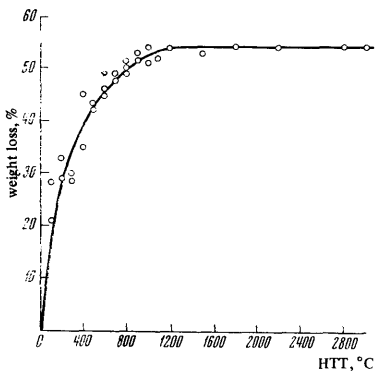


Figure 1. Change in weight of FPFR during heat treatment [42].

The greatest changes occur in the range 80–120°, and effectively cease at 180°. This is because the hardening process occurs mainly over the range 150–180° (as shown by chemical analysis).

Table 1. Composition changes during heat treatment of FPFR.

HTT, °C	Elemental analysis, %				HTT, °C	Elemental analysis, %			
	C	H	N	O		C	H	N	O
No heat treatment	68.26	5.68	4.40	21.66	500	82.39	4.65		
40	68.58	5.52			600	85.68	3.18	3.30	7.86
70	70.18	5.64	4.36	19.82	700	87.68	2.42		
80	70.16	5.59			800	91.29	1.52	2.84	4.35
100	70.88	5.61			1000	96.01	0.79	1.92	1.28
120	73.14	5.53			1100	96.98	0.53	—	—
150	73.24	5.50	4.54	16.72	1200	97.60	0.46	1.84	0.10
200	73.31	5.37	4.64	16.68	2000	98.29	0.23	—	—
300	74.33	5.40			3000	99.25	0.11	—	—
400	80.48	4.50	3.32	11.70					

The hardening process is controlled by a number of factors. In particular, the course of the hardening reaction is determined not only by temperature, but also by the heating rate and the duration of heat treatment. Higher heating rates tend to slow down the hardening process, to lower the proportion of insoluble fraction, and to increase the content of free components in FPFR. Polymers produced by heating the resin to 120° at different rates (1 and 30 deg h^{-1}) showed hardening factors of 89 and 81% respectively, and different contents of free furfural (5 and 10%) and of free phenol (0.9 and 1.3%). The experimental results of Fig. 2 show the variation of the degree of hardening with time of isothermal heating at different temperatures. The hardening time decreases on raising the temperature. Thus, a 10-hour heat treatment at 100° is needed to give 83% of insoluble fraction, as compared with only 5 h at 110°. Thus, the effect of temperature on the degree of hardening can be compensated to some extent by change in reaction time. The 150° curve is the steepest for times below 0.5 h and the flattest above 5 h. This shows not only that the reaction rate increases with hardening temperature, but also that the reaction at this temperature goes effectively to completion in a shorter time than at the other temperatures (120°, and below).

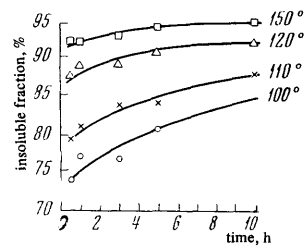


Figure 2. Percentage of insoluble fraction during hardening of FPFR under isothermal conditions [41].

An analysis of the volatile products evolved during hardening detected mainly furfural (95–96%), with a small amount of phenol, in the liquid condensate. The amount of condensate evolved is determined by the heating rate. Thus, on raising the rate from 10 to 40 deg h^{-1} the volume of condensate increases by a factor of 2 (from 20.8 to 42.2%). Hence we may conclude on the one hand that the heating rate determines the yield of polymer, and on the other hand that under these conditions the hardening of the material is due not only to chemical changes but also to the evolution of volatile fractions.

It is well known that many complex processes take place during hardening of phenol–formaldehyde resins [43]. Many workers believe [44–47] that a free-radical mechanism is involved.

The experimental results reproduced in Fig. 3 show the change in the concentration of paramagnetic centres (PMC) during hardening of the resin at temperatures up to 200°. The total number of PMC begins to increase appreciably at 70–80°, and continues to increase up to 120°. An arrest is observed over the range 120–150°, followed by a further increase in the number of PMC. The presence of a significant number of PMC in the original resin, decreasing during the initial heating period (below 70°) suggest that oxidation is occurring. This is confirmed by the fact that when the initial, pure novolac resin is allowed to stand in contact with the air for a long time its viscosity increases, and a fairly large ESR signal can be detected, whereas no such change occurs if the resin is stored out of contact with the air. The paramagnetism in this case may arise from peroxidic or quinonoid radicals formed by the oxidation of terminal groups of the resin molecule, which are also the most readily accessible to oxygen.

It should be noted that the hardened samples were very insensitive to atmospheric oxygen. The reported PMC concentrations relate to measurements in ordinary air.

It is evident from Fig. 3 that the number of PMC begins to increase when the temperature of heat treatment is greater than 70°, and becomes constant at 120–150°. On the other hand, chemical analysis indicates that the interaction between the components (i.e. the hardening process) continues to take place even in this range of temperatures. For example, the proportion of free phenol and furfural decreases gradually throughout the range of heat treatment temperatures. The i.r. spectra of the resin during hardening lead to the same conclusion. Experimental i.r. spectral data for the initial resin and for the material in various stages of hardening are shown in Fig. 4.

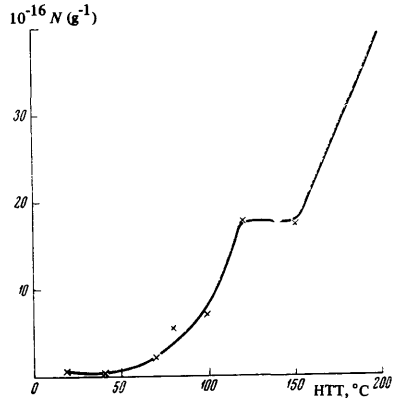


Figure 3. Formation of PMC during hardening of FPFR[42].

Heat treatment at 90° causes a large decrease in the intensity of the absorption band at 1660 cm^{-1} and almost complete disappearance of the 1570 cm^{-1} band. Both these bands arise from the furfural[48]: hence the changes may be explained either by a decrease in the amount of free furfural in the sample, or by volatilisation of this component, or by structural changes. The band at 1570 cm^{-1} is due to vibrations of the diene bonds in the furan ring which are conjugated with a carbonyl group. Hence, its disappearance may be ascribed to a decrease in the number of these bonds or to a decrease in the number of C=O groups (confirmed by the changes in the 1660 cm^{-1} band), or to the opening of one of the C=C bonds.

After heating the sample to 120°, the following changes are noted in the i.r. spectra. The band at 690 cm^{-1} (assigned to monosubstituted benzene rings, i.e. free phenol) disappears completely. The vibrations of the phenolic OH groups also give rise[49] to the bands at 1370 and 1200–1230 cm^{-1}, whose intensity decreases very significantly after heating the sample at 120°. The type of substitution of the benzene rings does not change (bands at 800–700 cm^{-1}), as shown also by the constant intensity of the 1600–1500 cm^{-1} bands which are very sensitive to the type of substitution. The number of aldehyde groups does not change (since the band at 1660 cm^{-1} is unchanged).

The absorption band of novolac at 1370 cm^{-1} is usually ascribed to vibrations of the phenolic hydroxyls. One of the furfural bands occurs at the same frequency. The 1370 cm^{-1} band disappears almost completely at 120°. It follows that the phenolic hydroxyls are involved in the hardening reactions. The nature of the bands in the 900–700 cm^{-1} region suggests that the benzene rings are not highly substituted[50,51]. No tetrasubstituted rings are detected by i.r. absorption. The narrow band at 880 cm^{-1}, which is characteristic of furans, shows that some of the five-membered rings survive the reaction.

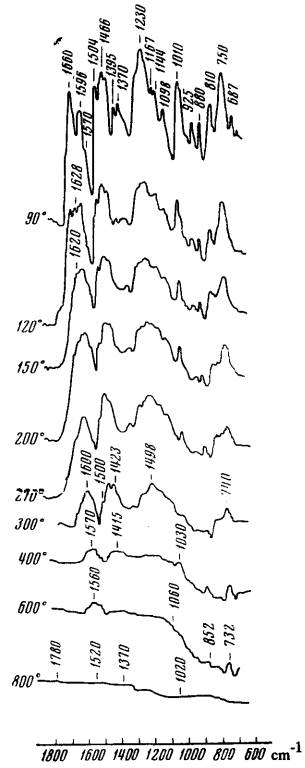


Figure 4. Infrared absorption spectra of FPFR after various stages of heat treatment[41,47].

A particularly interesting band, at 1628 cm^{-1}, can be due either to isolated C=C double bonds or to C=C double bonds conjugated exclusively with the carbonyl group or exclusively with the aromatic nucleus (without conjugation to another C=C bond).

After heat treatment to a higher temperature (150°), the absorption band of the aldehyde carbonyl group (1660 cm^{-1}) is no longer detectable. The strongest band is at 1620–1630 cm^{-1}. The 1370 cm^{-1} band (phenolic hydroxyls) has disappeared completely. The absorption bands associated with the furan ring are weaker, particularly the 930 cm^{-1} band from monosubstituted furan. Changes can be detected in the intensity of the 900–700 cm^{-1} band, and that of the 740–750 cm^{-1} band also shows a marked change. This latter band corresponds to the vibrations of the unsubstituted hydrogen in *ortho*-substituted benzene rings and in monosubstituted benzene and furan rings. The intensity

of absorption in the trough between the bands at 740 and 810 cm^{-1}, due to the formation of di-*ortho*-substituted rings, begins to increase at 150°.

The 1010 cm^{-1} band (from the C–O–C group) is the only furfural band still clearly visible in the spectrum at 200°. The 770 cm^{-1} band (triply substituted rings) is sharply resolved. At 870–880 cm^{-1} we observe a broad absorption band apparently due to the formation of 4-substituted benzene rings. The intensity changes in the region of 1600–1500 cm^{-1} are also interpreted in terms of changes in the type of substitution.

Thus, an analysis of these experimental results suggests that the hardening process occurs mainly in the range 70–150°, and that the process is characterised by a change in the number of PMC. The point at which the concentration of PMC begins to increase, and the point at which it becomes constant, can be identified with the initial and the final hardening temperature. The increase in the concentration of PMC is due to the formation of random molecular networks with a large number of broken cross-linking bonds.

The constancy of the concentration of PMC between 120 and 150° (Fig. 3) is evidently the result of the hardening of the resin to a solid product (of relatively low hardness). Isothermal heating in this temperature range produces only a slight consolidation of the three-dimensional network without forming any new PMC. These conclusions are consistent with the results of chemical analysis, which indicate that most of the free components of the resin have reacted chemically, and they are consistent also with the observed i.r. spectral changes.

In particular, the 1660 and 1370 cm^{-1} bands disappear almost completely at 150°. The most important band is found at 1620–1630 cm^{-1} (double bonds).

The increase in the concentration of PMC at temperatures above 150° is probably caused by pyrolysis of the resin.

The rate of hardening of the resin plays an important part in the formation of PMC. Thus, increasing the heating rate has been found to lower the concentration of PMC (from $\sim 2 \times 10^{17}$ spins g^{-1} at 5 deg h^{-1} to $\sim 0.7 \times 10^{17}$ spins g^{-1} at 20 deg h^{-1}). Evidently, a slow rise in temperature favours both a more complete chemical reaction between the components and the breaking of cross-linking bonds by pyrolytic action.

Isothermal heating at a temperature close to the upper hardening temperature does not alter the concentration of PMC appreciably. Thus, the number of spins was found to be 2×10^{17} and 2.5×10^{17} g^{-1} after heating at 120° for 1 h and 10 h respectively. These results are evidence that hardening occurs in a relatively short time.

The processes which occur during pyrolysis of hardened FPFR are particularly interesting[47]. The structural changes occurring during pyrolysis of the resin are reflected by changes in the i.r. spectra. It can be seen from Fig. 4 that heat treatment at 270° produces a sharp change in the intensity of the 1620–1630 cm^{-1} band. The band at 740 cm^{-1} becomes weaker, showing that the number of disubstituted rings has decreased. At the same time, sharp bands appear at 860 and 770 cm^{-1}, indicating more extensive substitution. The bands associated with the furan ring disappear, except the 1010 cm^{-1} band (C–O–C group). A band at 1260 cm^{-1} is clearly resolved in the region of 1200–1250 cm^{-1}. This band is found in all compounds containing C–O groups: it is often ascribed to aromatic ethers. Since the 1010 cm^{-1} band has not disappeared, any partial bonding of the C–O–C group (or –O–) to unsaturated carbon atoms should give rise to this band. It is difficult to account for the appearance of a broad line at 1600 cm^{-1}, and to decide whether this line is due to the aromatic ring only or whether it is conjugated with lines from C=C bonds.

At 300° all the furan bands have disappeared, including the 1010 cm^{-1} band. The i.r. spectrum now contains only bands associated with vibrations of aromatic rings (1600, 1500, and 740–800 cm^{-1}), and also bands from oxygen-containing groups (1250–1100 cm^{-1}).

After heat treatment at 400°, the oxygen content of FPFR is drastically reduced: all lines in the region 1250–1100 cm^{-1} have disappeared. The i.r. spectrum contains only an absorption band due to double bonds (mainly aromatic) at 1600–1500 cm^{-1}. The extent of substitution increases, as shown by the relatively strong band at 860 cm^{-1}. This effect may be due to condensation of the aromatic rings. The 1415 cm^{-1} band, due to residual $-CH_2$ groups, disappears completely at 600°.

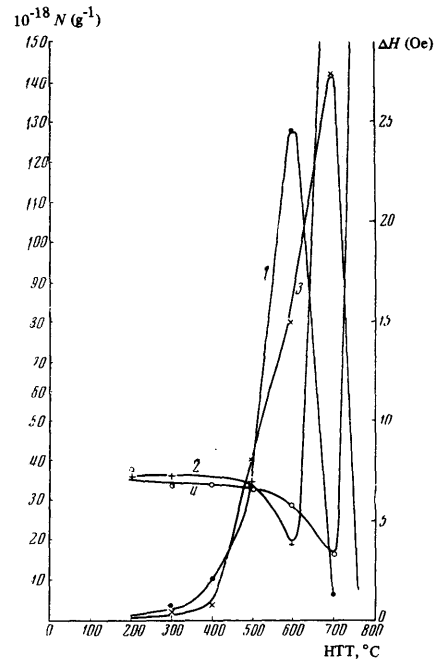


Figure 5. Concentration of PMC (N) and line width (ΔH) as a function of HTT[47]: *1*) and *3*) changes in N for samples heated at 5 and 20 deg h^{-1} respectively; *2*) and *4*) changes in ΔH for samples heated at 5 and 20 deg h^{-1} respectively.

The structural changes in the resin during heat treatment (HT) at temperatures above 200° (Fig. 5) result in changes in the concentration of PMC (curve *1*) and in the line width ΔH (curve *2*). The maximum ESR absorption is found at 600°, a temperature which is characteristic of carbonised substances. According to Trostyanskaya and coworkers[52], the highest concentration of PMC during pyrolysis of phenol–formaldehyde resins occurs in the range 400–500°. Others[53] have found a strong maximum at ~ 700° and smaller maxima in the region 1400–1800° and ~ 2800°. It follows that the position and the strength of the maximum are critically dependent on the type of resin.

The results of Fig. 5, obtained with samples in a vacuum, show that the total number of PMC increases slowly in the range 150–300°. Evidently, the growth in the concentration of PMC in this case denotes onset of pyrolysis, elimination of oxygen-containing groups and low-molecular-weight products, and dissociation of the dimethylimino bonds formed during the curing. The range 300–500° is characterised by a sharp increase in the concentration of PMC, due to the intensification of the above reactions and to the formation of aromatic molecules with unpaired electrons. This is confirmed by the analytical results (Table 1), which show that the most extensive changes in composition occur at temperatures ≥ 300°.

However, the carbonised product still contains a fairly large amount of nitrogen (1.8%) and a trace of hydrogen (0.5%). Thermal dehydrogenation, which sets in when the resin is heat treated above 400°, also contributes to the evolution of hydrogen from the sample (as shown by the results of chemical analysis). This process is partly responsible for the decrease in line width (ΔH) in the temperature range 500–600°, associated with the loss of hyperfine interaction (see curve *2* of Fig. 5). The main line-broadening mechanism in this temperature range, in addition to spin–spin interaction, is probably spin–orbit coupling, as suggested by the strong temperature dependence of the spin–lattice relaxation time. The spin–lattice relaxation time of a resin heat-treated at 600° is approximately an order of magnitude larger than for the same material at room temperature.

However, since the sharp rise in concentration of PMC is accompanied by a relatively small change in ΔH, it may be assumed that different types of paramagnetic centre exist in different regions.

The mechanism of thermal degradation of the resin has been elucidated by measuring the yield of gas as a function of temperature and time (Fig. 6). The composition of the gas is different for different temperature ranges. The strongest gas evolution occurs at 600–800°, the range where the degradation processes are most marked. On further raising the temperature there is a large decrease in the amount of gas evolved.

The degradation process begins to slow down after 25–30 min under isothermal conditions in the temperature range 200–1000° (Fig. 6).

The ESR absorption maximum observed at 600° corresponds with the temperature of maximum gas evolution (Fig. 5). This is evident from the composition of the gases evolved during pyrolysis.

As the pyrolysis temperature is raised, the composition of the gases evolved changes continuously (Table 2). The gas resulting from pyrolysis at 200–500° consists mainly of CO and CO_2. Significant amounts of methane are evolved at 500–800°, with a maximum at 600°, and at the highest temperatures the concentration of methane falls to 3%. The largest change was observed in the hydrogen concentration, which increased to 87% when the temperature was raised to 1000°.

Evidently, pyrolysis of methane can occur at the higher temperatures. The concentration of CO decreases continuously from 46 to 5%, and that of CO_2 from 52 to 3%.

The formation of volatile products by low-temperature pyrolysis is probably associated with the opening of heterocyclic rings, whereas at the higher temperatures (but below 800°) the mechanism is probably dehydrogenation of benzene rings.

The position of the ESR absorption maximum during carbonisation is determined not only by the type of resin but also by the heat-treatment regime. Fig. 5 shows the changes in concentration of PMC and in line width ΔH for a resin subjected to different heating rates (5 deg h^{-1} for curves *1* and *2*, 20 deg h^{-1} for curves *3* and *4*). It is clear that the concentration maximum and the ΔH minimum are shifted towards higher temperatures (▷ 700°) when the heating rate is changed from 5 deg h^{-1} to 20 deg h^{-1}.

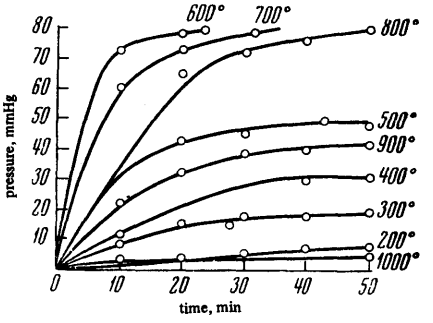


Figure 6. Yield of gas during pyrolysis of FPFR under isothermal conditions at different temperatures[47].

These effects can be understood on the assumption that bond breaking and thermal dehydrogenation (and the resulting structural rearrangements) cannot be fully effective if the heat-treatment temperature (HTT) is allowed to rise above 400° too rapidly.

Table 2. Composition of the gaseous pyrolysis products of FPFR[47].

HTT, °C	Components, expressed as vol.% of total gas evolved					
	CO	CO_2	CH_4	H_2	H_2O	Remarks
200	46	52	—	—	—	2% ($O_2 + N_2$)
300	59	37	—	—	—	4% ($O_2 + N_2$)
400	57	41	2	—	—	—
500	40	38	18	2	—	2% ethylene–ethane
600	19	10	45	26	—	—
700	17	2	38	43	—	—
800	8	2	20	68	2	—
900	6	3	5	84	2	—
1000	5	3	3	87	2	—

The decrease in concentration of PMC when the resin is heat treated above 600° is due to the loss of aromatic hydrogen and to the disappearance of free radicals which accompanies the formation of aromatic structures. The decrease in spin–lattice interaction time, leading to an increase in ΔH, is consistent with this hypothesis. The absence of ESR absorption for HTT > 700° (Fig. 5) is ascribed to incipient ordering of the resulting two-dimensional structure. As a result, the electrical conductivity of the sample begins to increase rapidly. It should be noted that the temperature at which ESR absorption begins to disappear is a characteristic of the particular resin: all the properties of the material begin to change at this HTT. Thus, the hardness and the density show a sharp increase, and the electrical resistivity begins to fall off very rapidly.

Studies of the influence of atmospheric oxygen on the PMC of a carbonised resin have yielded very interesting results. The relative sensitivity to atmospheric oxygen of the PMC in samples which have been exposed to different heating rates is illustrated in Fig. 7. Two regions where the effect of oxygen is large can be clearly seen. Thus, the ratio N_{vac}/N_{air} remains constant in both cases over the range 300–500°. The concentration of PMC also changes very little on heating the resin to 400°. This is because the rate of pyrolysis is very low in this range of temperatures, and the total number of PMC is small. The effect of oxygen becomes significant for HTT above 450°, and the maximum of the N_{vac}/N_{air} ratio coincides with the maximum PMC concentration in both cases. In both regions, the effect of oxygen is stronger when the sample is heat treated by the slower regime (Fig. 7). These experimental results justify the conclusion that the difference in sensitivity to atmospheric oxygen is associated with the extent of the structural changes in the resin, which are less extensive when fast heating rates are used. Hence, the PMC formed during fast heating of the resin are less sensitive to oxygen.

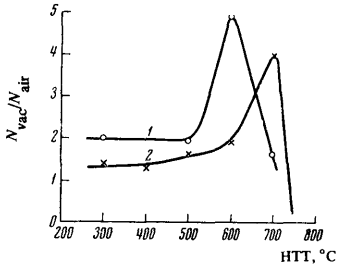


Figure 7. Relative sensitivity of the PMC to oxygen[47]: *1*) heating rate 5 deg h^{-1}; *2*) heating rate 20 deg h^{-1}.

The interaction of atmospheric oxygen with PMC is probably influenced by the oxygen chemically bound in the resin structure. For example, the fact that curve *2* in Fig. 7 has a lower maximum than curve *1* is probably explained by the presence of bound oxygen atoms in the pyrolysis products obtained at 600–700°. Even with the slower heat-treatment regime (5 deg h^{-1}), the products contain 7.86% of oxygen (Table 1). Oxygen atoms chemically combined in the carbonised samples can screen them from the effect of atmospheric oxygen.

Indirect confirmation of this hypothesis is provided by the measured spin–lattice relaxation times for pyrolysis at 600° (1.1×10^{-4} s for a heating rate of 5 deg h^{-1} and 0.12×10^{-4} s for a heating rate of 20 deg h^{-1}). It is well known that the presence of oxygen can lead to shorter relaxation times. The difference in the effect of oxygen on the PMC concentration for fast and for slow heating rates probably stems from differences in the degree of delocalisation of the unpaired electrons.

The presence of regions of different sensitivity may be partly due to the formation of different types of radical, with different reactivities towards oxygen, during the various stages of isothermal heating. This is confirmed by ESR measurements over a range of temperatures. For an HTT of 500°, corresponding to the onset of sensitivity to oxygen, the temperature dependence of the ESR absorption signal shows marked deviations from Curie's law.

III. PROPERTIES OF VITREOUS CARBON

1. Physical and Mechanical Characteristics

The properties of vitreous carbon of different origins (Japanese, French, and Soviet) are listed in Table 3[2–4,18,54]. The preparation of these materials is described in Ref. 55–59. The Table also lists, for comparison, the properties of a number of other materials: cellulose carbon, quartz, glass, high-density impregnated graphite, and ordinary graphite.

It is important to note that the properties of vitreous carbon can show wide variations, depending on the heat-treatment regime. Materials with different physical and mechanical characteristics can be prepared from a single carbonaceous starting material.

Vitreous carbon remains a solid up to 4000°K, and its properties are unchanged up to some temperature close to the sublimation point[60]. Its density is relatively low (up to 1.5 g cm^{-3}) in comparison with most refractory elements and compounds. Vitreous carbon is much harder than the common industrial grades of artificial graphite.

The elastic modulus of vitreous carbon is also higher than the modulus of the common graphitic materials (1500–3100 kg mm^{-2}, as compared with 300–800 kg mm^{-2} for industrial graphite).

The hardness of vitreous carbon is very sensitive to the maximum HTT of the material.

Kotlensky and Martens[61,62] showed, in their study of the mechanical properties of carbonaceous materials, that the strength of vitreous carbon (of any grade) is much higher than the strength of materials prepared from coke and pitch, but lower than the strength of pyrolytic graphite in a direction parallel to the deposition plane.

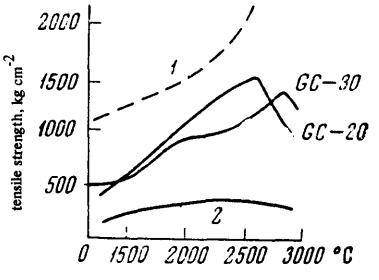


Figure 8. Tensile strength as a function of temperature[62]: *1*) pyrolytic graphite; *2*) graphitised material from pitch and coke. GC-20 and GC-30 are vitreous carbons heat treated at 2000 and 3000° respectively.

The strength of vitreous carbon is influenced by temperature (Fig. 8). The tensile strength of GC-20 vitreous carbon increases with temperature, reaching a maximum of 1400 kg cm^{-2} at 2500°.[62] At still higher temperatures

Table 3. Properties of different grades of vitreous carbon and other materials.

Property	Soviet vitreous carbon Ref.(18)			Japanese vitreous carbon Ref.(4)			French vitreous carbon Ref.(54)		Cellulose carbon tubes Ref.(4)	Transparent quartz Ref.(4)	Borosilicate glass Ref.(3)	Impregnated graphite Ref.(4)	High-density graphite Ref.(2)	Ordinary graphite Ref.(2)
	SU-12	SU-20	SU-30	GC-10	GC-20	GC-30	V 10	V 25						
Max. working temp. (°C) in an inert or reducing atmosphere or in vacuum	1200	2000	3000	1300	2000	3000	1000	2500	2500	1670	500	1300	3000	3000
Apparent density (g cm^{-3})	1.47—1.55	1.38—1.48	1.06—1.27	1.47—1.50	1.46—1.47	1.43—1.46	1.5—1.55	1.50—1.55	1.48	2.2	2.23	1.75—1.92	1.7—1.9	1.5—1.6
Open (apparent) porosity, %	0.2—1.3	0.7—2.0	1.8—2.2	0.2—0.4	1—3	3—5	0	0	—	—	—	8—15	10—20	25—35
Gas permeability (cm^2 s^{-1}) at room temperature	$\leqslant 10^{-8}$	$\leqslant 10^{-8}$	$\leqslant 10^{-8}$	10^{-11}—10^{-12}	10^{-10}—10^{-12}	10^{-7}—10^{-9}	$\leqslant 10^{-10}$	$\leqslant 10^{-8}$	10^{-12}	10^{-10}—10^{-12}	10^{-10}—10^{-12}	10^{-5}—10^{-6}	10^{-1}—10^{-2}	10^{0}—10^{-1}
Shore hardness	—	—	—	110—120	100—110	70—80	120—125	120—125	—	—	—	45—55	—	—
Microhardness, kg cm^{-2}	150—230	110—170	70—80	—	—	—	225	150—175	—	—	—		—	—
Bending strength, kg cm^{-2}	2600—3200	2100—2400	2100—2400	900—1000	700—800	400—500	1000	600—800	—	400—800	400—800	400—500	200—500	100—180
Electrical resistivity, ohm mm^2 m^{-1}	45—54	45—54	45—54	45—50	40—45	30—35	55	45	45	10^{19}	10^{11}	9—11	—	—
Ash content, %	0.01—0.05	0.01—0.05	0.01—0.05	0.1—0.2	0.1—0.2	<0.05	0.02	0.005	—	—	—	0.1—0.2	—	—
Thermal conductivity, kcal m^{-1} h^{-1} deg^{-1}	—	—	—	3—4	7—8	13—15	—	—	—	—	0.5—1.0	100—120	100—120	100—120
Thermal expansivity, $\times 10^6$ (deg^{-1})	4.6—5.8*	4.6—5.8*	3.7—5.7*	3.2—2.2	2.0—2.2	2—2.2	3.2	3.2	2.5	0.3	3.2	2—2.5	2—2.5	2—2.5
Elastic modulus, kg mm^{-2}	2800—3100	2300—2700	1500—1700	2700—3000	2500—2900	1500—2000	2850	2200	2700	7780	7000	1000—1200	500—800	300—600

* The measurements for grades SU-12, SU-20, and SU-30 were made at 1200, 2000, and 3000°C respectively.

the tensile strength begins to fall off, as in the case of most graphitic carbons prepared by traditional methods. In GC-30 vitreous carbon the tensile strength also increases as the temperature is raised from 1900 to 2700°, but it is lower than the strength of GC-20 over most of the range of temperatures. It is not clear from the data whether the tensile strength of GC-30 reaches a maximum at 2700° or whether it continues to increase with temperature.

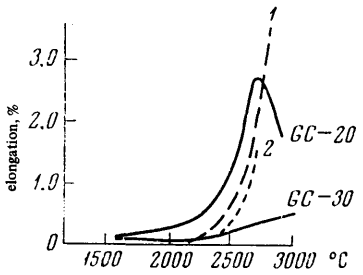


Figure 9. Elongation at break as a function of temperature[62]: *1*) pyrolytic graphite; *2*) graphitised material from pitch and coke. GC-20 and GC-30 are vitreous carbons heat treated at 2000 and 3000° respectively.

At temperatures of the order of 2200° and below the elongation at break of vitreous carbon (Fig. 9) is less than 3%, i.e. of the same order as for materials prepared from pitch and pyrolytic carbons. At 2500° the elongation of GC-20 increases much more drastically than that of the other materials. The increase continues as far as 2700°, and the elongation remains much greater than that of pitch-carbon materials and slightly higher than that of pyrolytic graphite. In GC-30 vitreous carbon the deformation at break is smaller than in GC-20 and other graphitic carbon materials.

Table 4. Properties of different grades of vitreous carbon before and after deformation.

Property	Grade GC-20		Grade GC-30	
	initial	deformed*	initial	deformed**
Density, g cm^{-3}				
In air	1.50	1.29	1.50	1.44
In light petroleum	1.68	1.82	1.68	1.66
Elementary cell parameters, A				
c	7.00	6.85	6.84	6.86
a	2.43	2.43	2.45	2.44

* Sample was deformed by 33% at 2700°.
** Sample was deformed by 65% at 2700°.

The properties of vitreous carbon before and after deformation are listed in Table 4. In contrast to the normal graphitic carbons, vitreous carbon has practically identical properties in different directions[15]. Nakamura and coworkers[63] conclude that vitreous carbon remains isotropic even when it contains small additions of natural or synthetic graphite.

Materials with graphite additives do not differ appreciably in density, hardness, and elastic modulus after heat treatment at 1300 and 2000°. Materials of the same grade, but heat treated at 3000°, have very different properties. A likely explanation is that the presence of graphite assists graphitisation at temperatures above 2000°.

Fischbach[64,65] studied the strength and elongation at break of vitreous carbon samples as a function of temperature, and found that an initially isotropic material becomes anisotropic after deformation. This suggests reorientation of the crystallites in a direction parallel to the strain axis.

Unlike silicate glasses, vitreous carbon has a very high thermal stability. No change could be detected after many fast heating and cooling cycles between 1700° and room temperature[22]. Similar results were obtained after ten cycles of instantaneous heating to 2000° in a stream of nitrogen and quenching to room temperature (after one minute) in carbon powder, and after five cycles of heating to 1000° and quenching in cold water[66]. In this respect, vitreous carbon is superior even to fused alumina.

2. Electrical and Semiconducting Properties

Vitreous carbon is an electrical conductor, but its resistivity is higher than that of the usual grades of graphite and of the same order as that of the carbon-black grades of artificial graphite.

Barykin and coworkers[27], and also a number of foreign workers[67,68], have studied electrical conduction in vitreous carbon and have observed semiconducting properties over a wide range of temperatures.

Yamaguchi[67] measured the Hall coefficient, magnetoresistance, and electrical conductivity of vitreous carbon as a function of heat-treatment temperature (from 1000 to 3200°) and at different temperatures (20, 77, and 330°K). Two types of sample were investigated: impervious (i.e. glassy) and porous (Fig. 10), both prepared from the same starting material. For low heat-treatment temperatures the Hall coefficient of both samples varied with HTT in the same way: it was positive for HTT around 1000°, it became negative (going through a minimum at ~ 1400°) on raising the HTT, and again changed sign becoming positive at ~ 1600° HTT.

In the region of high heat-treatment temperatures the two samples behaved differently: whereas the Hall coefficient of vitreous carbon increased with HTT up to 3200°, without going through a maximum, the Hall coefficient of the other type of sample went through a broad maximum at a heat-treatment temperature of ~ 3000°, and began to fall off beyond that temperature.

The Hall coefficient of both types of sample was much lower than typical values for graphitised materials over the whole range of HTT. At lower measurement temperatures the maximum in the Hall coefficient curve for the second type of sample was shifted towards higher HTT. The Hall coefficient of vitreous carbon was independent of measurement temperature over the whole range of HTT.

The variation of magnetoresistance with HTT was very different for the two types of sample. In vitreous carbon the magnetoresistance was negative, and decreased on raising the HTT. In the second type of sample the magnetoresistance became positive after going through a minimum, and continued to increase rapidly beyond that point.

From these results, the authors conclude[67] that the graphitisation tendency of the two types of sample is differ-

ent: whereas the second sample begins to graphitise at high HTT (~ 3000°), the vitreous sample shows no sign of graphitisation even at a HTT of 3200°.

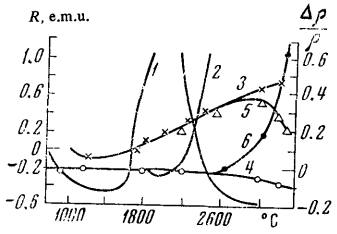


Figure 10. Hall coefficient (R) and magnetoresistance ($\Delta\rho/\rho$) as a function of HTT (measurements at 300°K)[68]. Samples of graphitising material: *1*) R, *2*) $\Delta\rho/\rho$; samples of the first type: *3*) R, *4*) $\Delta\rho/\rho$; samples of the second type: *5*) R, *6*) $\Delta\rho/\rho$.

Yamaguchi ascribes the inability of vitreous carbon to undergo graphitisation to specific structural features of this material. He believes that the second type of sample was structurally inhomogeneous, and that only some isolated regions of the material were able to undergo graphitisation.

Table 5. Pore size distribution in graphitic materials[16].

Material	Pore volume, Å	% or pores in range			Maximum pore size at pressure ≤ 1000 kg cm^{-2}, Å
		$7\cdot10^3$—$7\cdot10^4$, Å	$1\cdot10^3$—$7\cdot10^3$, Å	$1\cdot10^2$—$1\cdot10^3$, Å	
Ordinary graphite	32	27	4	3	$7\cdot10^4$
High-density graphite	11	3.5	1.5	6	$7\cdot10^4$
Impregnated graphite	5	—	2.5	2.5	$7\cdot10^3$
Vitreous carbon	0.35	—	—	0.35	$1\cdot10^3$

The thermoelectric power and Hall coefficient have been measured by Tsuzuku and Saito[69,70] as a function of measurement temperature and HTT. The observed change of the type of current carrier from holes (p-type) to electrons (n-type) and again to holes is interpreted in terms of Mrozovskii's σ-trap model of the electronic structure of the normal soft forms of carbon.

No definite theory of the electronic structure of vitreous carbon can be based on the above results.

3. Pore Structure

The microstructure of vitreous carbon differs drastically from that of graphite (both ordinary and impregnated[16]). The specific, granular pore structure of ordinary graphitised materials is not found in vitreous carbon.

The pore distribution in vitreous carbon, as measured with a mercury porosimeter, also differs from that of ordinary graphite (Table 5).

The most important characteristic of the new material is its low permeability to gases. Davidson[15] measured the permeability of cellulose carbon using tubular samples with 5.08 mm wall thickness. The samples were exposed externally to a helium atmosphere, the inner volume was carefully evacuated, and the tubes were connected to a diffusion pump and helium mass-spectrometer. The permeability of the material was well below 10^{-12} cm^2 s^{-1}. The permeability of vitreous carbon does not change with time: a diaphragm of this material mounted between a vacuum and helium at 1 atm pressure did not change significantly in the course of 700 hours. Other experiments showed that the material remains impervious at elevated temperatures (1000°).

The permeability of vitreous carbon can also be investigated by the density method. An impermeable material should have the same density in different media.

Table 6 lists the measured densities of vitreous carbon for different heat-treatment temperatures and in different media. Density was measured by the ordinary pyknometric method, and also in mercury and in helium[15].

Table 6. Density of vitreous carbons with different HTT in different media[20].

Heat-treatment temp., °C	Density, g cm^{-3}		
	pyknometric	in mercury	in helium
950	1.55	1.53	1.95
1200	1.61	1.59	1.66
1500	1.58	1.58	1.61
2000	1.55	1.56	1.58
2500	1.48	—	—

It is clear from the results of Table 6 that after heat treatment at 950° the pyknometric density of vitreous carbon (1.55 g cm^{-3}) is not the same as the density measured in a helium pyknometer (1.95 g cm^{-3}). The higher value of the density against helium suggests the presence of open pores.

Further heat treatment of the vitreous carbon causes the helium density to decrease to the level observed in the other media, i.e. it produces a closed pore structure. It is assumed that the formation of an isolated pore structure is due to the growth of separate crystallites during heat treatment (the pore diameter being small and comparable with the size of the crystallites). Diaphragms are formed within the pores, and the material becomes impervious to gases.

Intensive studies of helium density as a function of heat treatment temperature and X-ray studies by the low-angle scattering method have shown that the pores in vitreous carbon have extremely small dimensions. By comparing helium density data with low-angle scattering data Davidson concludes[15] that the average pore diameter is ~ 20 Å.

4. Crystal Structure

X-ray analysis has shown that vitreous carbon is a typical non-graphitising material[3].

The crystals in vitreous carbon, ~ 100 Å in diameter, do not have three-dimensional order. The crystallites are separated by voids and by chains of atoms without any particular orientation[5]. The degree of graphitisation of

GC-30 vitreous carbon is about the same as in petroleum carbon heated to 1900°.

Whereas in graphitised materials the interplanar spacing decreases gradually to 3.35 Å as a result of heat treatment, in vitreous carbon this value is constant (3.4 Å) even when the graphitisation temperature is raised above 3000°. Crystallographic studies of the new material have shown that the final product does not contain any large crystals. Well developed crystals are very seldom found, and their diameter is usually no more than a few hundred Ångstroms, whereas the average crystal size in natural graphites is at least 1000 Å.[42]

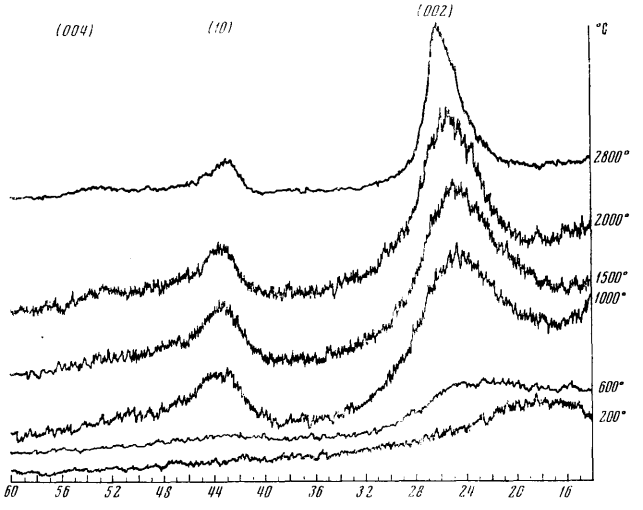


Figure 11. Diffractograms of carbonised FPFR products for different HTT[42].

X-ray diffraction patterns[42] for vitreous carbons heat treated at different temperatures are shown in Fig. 11. The diffraction patterns of the carbonisation products of the resin contain reflections of two types [(001) and (hk0)]. Diffuse (002), (004), (10), and (11) bands are observed in approximately the same angular position as the corresponding three-dimensional reflections from graphite. The (002) and (004) reflections arise from interference between groups of aromatic layers of condensed carbon atoms with sp^2 hybridisation of the valence electrons in the layer. The (10) and (11) bands are due to two-dimensional diffraction by flat layers[71].

A high background level is observed in the diffraction patterns of heat-treated samples. The large background arises from non-coherent scattering of the X-ray beams by carbon in non-aromatic configurations and by various radicals present as an amorphous phase.

On heating the starting material above 100°, complex structural changes take place. These consist mainly in breaking existing bonds and forming new ones, as shown by the diffraction patterns. At 200 and 600° the samples give an (002) diffraction line without a clearly defined maximum. The diffraction peaks from the (10) and (004) planes merge into a smooth curve, and cannot be resolved, suggesting lack of three-dimensional order. After heating at 1000° the (002) diffraction line is clearly visible, with a fairly sharp maximum. The asymmetric outline of the reflections indicates the presence of disordered networks in the heat-treated samples.

On raising the HTT, the following changes are observed: the layer spacing decreases, the layers of condensed aromatic carbon grow in size, the packets of flat hexagonal layers become thicker, and the proportion of amorphous phase decreases (Fig. 12).

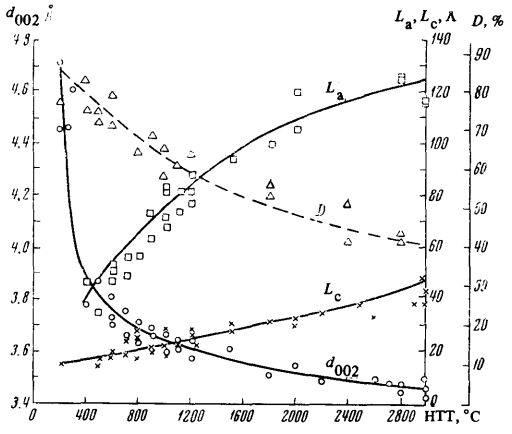


Figure 12. Interplanar spacing (d_{002}), crystallite size (L_a, L_c), and content of disordered phase (D) as a function of HTT in products obtained from FPFR[9].

The change of diamagnetic susceptibility of vitreous carbon with HTT also shows that this material is a typical non-graphitising carbonaceous material. Two regions can be distinguished in Fig. 13. For HTT between 200 and 1200° the diamagnetic susceptibility does not change very appreciably: it goes through an ill-defined minimum at 600–700°, and does not rise above the value -1.0×10^{-6} (CGSM units g^{-1}). At temperatures above 1300° the diamagnetic susceptibility begins to increase more rapidly, and the approximately linear increase continues up to 3000°.

The change in susceptibility with HTT in the low-temperature region is associated with changes in the molecular structure of the starting material, resulting from the polymer degradation processes. These processes involve the breaking of carbon–carbon bonds in macromolecules, and therefore give rise to a large number of unpaired, localised electrons. The appearance of unpaired electrons in a sample is detected as paramagnetism, due to the magnetic moments of these electrons, and this explains the decrease in the net diamagnetic susceptibility[72].

The fast growth of diamagnetic susceptibility at higher HTT is due to the increased size of the hexagonal carbon layers (not exceeding 150 Å, however). This is interpreted[73] as evidence of the end of the pre-crystallisation period. The diamagnetic susceptibility, unlike the susceptibility of well graphitised materials, does not saturate even at a HTT of 3000°. The susceptibility corresponding to this HTT is -5.1×10^{-6}, i.e. significantly different from the mean susceptibility of graphite (-7.2×10^{-6}).

The non-graphitising properties of vitreous carbon are probably due to the presence of a three-dimensional network of cross-linking bonds in the starting materials: this network hinders the rearrangement of structural elements which is the precursor of the formation of graphitic structures during heat treatment [74-77].

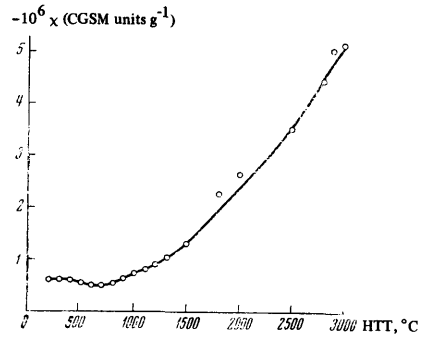


Figure 13. Magnetic susceptibility as a function of HTT [42].

As well as these purely structural effects, the presence of nitrogen atoms may affect graphitisation at temperatures above 1200°, because these atoms tend to hinder densification and the formation of ordered structures on heating.

Particles of different morphology have been detected in samples of SU-30 vitreous carbon by electron microscopy and selected-area electron diffraction [42]. Hence, graphitisation at high temperatures can take place heterogeneously, by evaporation and condensation of carbon atoms. The reason for the formation of morphologically different modifications in the products of high-temperature carbonisation is not clear.

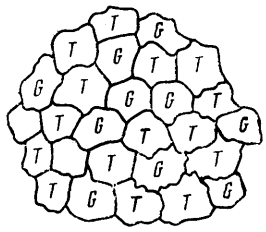


Figure 14. Structural model of vitreous carbon [77-79].

The regions of three-dimensional order, observed in microdiffraction experiments, must have a profound effect on the average structural parameters of the material.

Noda and Furukawa [78-80] studied the structure of vitreous carbon by measuring interplanar spacings, crystallite size, and the content of disordered regions, and also by radial distribution function analysis. Their results led them to a model of the structure of vitreous carbon involving two types of carbon: a tetrahedral modification, in which the arrangement of carbon atoms is similar to the diamond structure, and a trigonal modification, resembling graphite. The vitreous carbon may also contain carbon atoms with other types of bond.

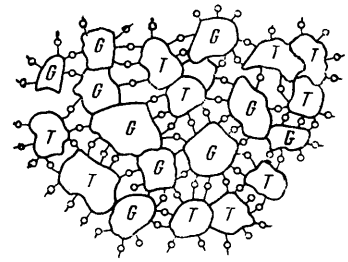


Figure 15. Structural model of vitreous carbon [77-79].

According to this structural model, the tetrahedral atoms (*T*) in vitreous carbon are responsible for most of the cross-linking bonds which hold together the graphitic layers (*G*) in a random arrangement (Fig. 14).

The model proposed for low-temperature grades of vitreous carbon, which are known to contain appreciable amounts of oxygen, involves oxygen bridges (Fig. 15) between *T* and *T*, *T* and *G*, and *G* and *G* regions.

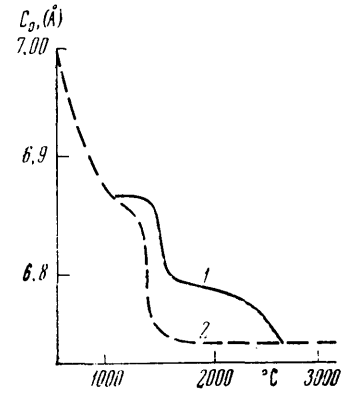


Figure 16. C_0 for GC-7 vitreous carbon (curve *1*) and for carbonised poly(vinyl chloride) (curve *2*) as a function of high-pressure HTT [81-83].

Kakinoki [81] suggests that the oxygen bridges can prevent the formation of ordered structures in vitreous carbon at temperatures up to 1200°, but they are broken down by heat treatment at 2500–3000°.

Noda and Cato [82,83] have shown that the dimensions of the crystal lattice in vitreous carbon can be modified by graphitisation under pressure. Fig. 16 shows the parameter C_0 of vitreous carbon (GC-7 grade) heat-treated under a pressure of 10 kbar and held at that pressure for 3 min.

For comparison, curve 2 gives the C_0 values for poly(vinyl chloride) carbon heat-treated under the same conditions.

The parameter C_0 falls to a very low value (6.72 Å) after heat treatment at 2600° under pressure. This low value of C_0 is not found in vitreous carbon prepared at ordinary pressure (C_0 for the GC-30 grade does not fall below 6.81 Å).

A possible explanation[84] is that the graphitic layers become mobile under pressure, and structural rearrangements towards more ordered structures become allowed.

In spite of the large number of published papers, our knowledge of the structure of vitreous carbon is still very inadequate.

5. Impurities in Vitreous Carbon

The specifications for construction materials used in many sectors of modern industry (nuclear energy, semiconductor technology, etc.) often include stringent purity requirements.

It is claimed[4] that the ash content of vitreous carbon does not exceed 0.02%. In the GC-30 grade, after additional purification, the ash content is decreased to ≤ 0.015%. Spectroscopic analysis results[2] for two grades of vitreous carbon (GC-20 and GC-30S) are summarised in Table 7. The following impurities are present: iron, aluminium, calcium, magnesium, silicon, vanadium, manganese, copper, and boron.

Table 7. Impurities in vitreous carbon[2].

Element	GC-20 before purification	$GC-30_S$	Element	GC-20 before purification	$GC-30_S$
Al	24.7	9.4	Mg	5.5	0.1
Ca	72.0	13.0	Mn	10.2	2.0
Co	none detected	none detected	Ni	none detected	2.6
Cr	none detected	none detected	Si	27.3	0.1
Cu	10	4.9	V	53.0	none detected
Fe	>100	>100	B	1	0.1

The impurity content of vitreous carbon is largely determined by the purity of the raw materials and by the temperature of heat treatment.

Lewis and coworkers[85] prepared semiconductor materials in containers made from vitreous carbon and from artificial graphite, and concluded that vitreous carbon is the better crucible material because it does not offer an open pore structure for the migration of impurities. Thus, the impurities present in vitreous carbon are less likely to contaminate the contents of the crucible than the impurities present in graphite.

6. Chemical Stability and Reactivity

Vitreous carbon is very stable towards many aggressive media. It is stable to fused alkalies and salts (sodium hydroxide, potassium bisulphite, calcium fluoride), acids (hydrochloric, hydrofluoric, nitric, sulphuric, chromic), and oxidising agents (bromine, chlorine, and mixtures of hydrogen peroxide and nitric acid and of nitric acid and potassium chlorate)[86,87]. Vitreous carbon is unaffected after two months in a mixture of concentrated HCl and HNO_3, which is known to disintegrate ordinary graphitic materials after 48 h at room temperature. The weight loss in mixed acids is acceptably low (see Table 8).

Outstandingly good anti-corrosion properties were reported also for vitreous carbon in contact with a mixture of nitric and hydrofluoric acid. However, vitreous carbon disintegrates in the presence of alkali metals. The behaviour of various grades of vitreous carbon in the presence of potassium vapour was studied by Halpin and Jenkins[88], who observed the formation of intercalation layers. Sodium vapour also caused disintegration of the vitreous carbon, but only at higher temperatures and with finely divided materials.

Table 8. Weight changes of vitreous carbon in oxidising media[66].

Oxidiser	Weight loss (%) after 50 days at 20 ± 5°		
	GC-10	GC-20	GC-30
98% H_2SO_4 + 60% HNO_3 (1:1 by vol.)	0.12—0.18	0.19—0.27	0.8—1.1
20% H_2SO_4 + 20% HNO_3 (1:1 by vol.)	0.03—0.06	0.19—0.20	0.5—1.2
60% HNO_3 + 35% HCl (1:1 by vol.)	0.04—0.05	0.12—0.15	0.01—0.02
20% HNH_3 + 20% HCl (1:1 by vol.)	0.03—0.10	0.12—0.14	0.05—0.06

Experiments on the interaction of vitreous carbon with fused alkali metal salts have shown that the extent of disintegration depends on the temperature and on the nature of the corrosive agent[89].

The oxidation of vitreous carbon by carbon dioxide has been studied in detail[7,90,91] because of its relevance to the use of vitreous carbon in CO_2-cooled atomic reactors. The conclusion was that vitreous carbon oxidises at about the same rate as reactor graphite if due allowance is made for the active surface areas of the two materials. This quantity depends on the parameters which determine the surface-to-volume ratio.

Table 9. Rate of oxidation of vitreous carbon in carbon dioxide[2].

HTT of vitreous carbon, °C	Experimental temp., °C	Gas pressure, atm	Rate of oxidation $\times 10^6$, $g\,g^{-1}\,h^{-1}$
2000	545±10	0.82	0.31
2300	545±10	0.94	0.27
1455	740±5	1.2	23.8
1620	740±5	1.12	6.6
1780	740±5	1.43	6.3
2000	740±5	1.05	3.0
2400	740±5	1.26	1.1
2010	785±10	0.49	1.79
2400	785±10	2.11	6.9

The rate of oxidation is affected by the gas pressure and by the temperature of heat treatment: it increases on raising the gas pressure and on lowering the HTT (Table 9). Addition of CO to the reaction medium lowers the rate of oxidation.

On raising the HTT from 1455 to 2400°, the reactivity of the vitreous carbon at 740° fell from 23.8×10^{-6} to 1.1×10^{-6} $g\,g^{-1}\,h^{-1}$. The reactivity decreases also at lower experimental temperatures.

Lewis [90] investigated the oxidation of vitreous carbon and pyrolytic graphite in different gases. The flow rate of the oxidising gas was 0.5 litre min^{-1} at temperatures below 800° and 1–1.5 litre min^{-1} above 800°. He concluded that vitreous carbon oxidises more slowly than various forms of pyrolytic graphite (Fig. 17).

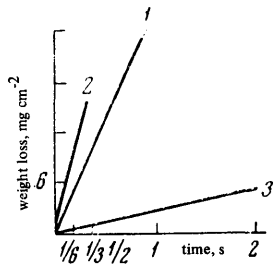


Figure 17. Weight loss of various graphitic materials as a function of time of oxidation in dry air at 750° [90]: *1*) purified graphite; *2*) not purified; *3*) vitreous carbon.

Yamada and Sato [16] studied the oxidation of vitreous carbon samples (15 × 15 × 1 mm) in a flowing mixture of nitrogen and oxygen in the ratio of 81 : 19 (by volume)at a temperature of 800 ± 5° and a flow rate of 0.5 litre min^{-1}. The results (Table 10) show that vitreous carbon is more stable towards oxidation than the other forms of graphitic material.

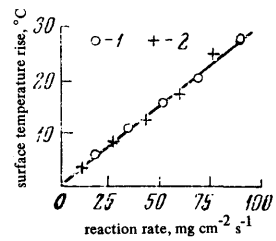


Figure 18. Rise in surface temperature as a function of rate of oxidation: *1*) vitreous carbon; *2*) graphite [90].

Blackman [91] observed the formation of isolated depressions on the surface of pyrographite and vitreous carbon during oxidation. He suggested that these craters are associated with the presence of metallic impurities, which act as oxidation catalysts, but this hypothesis is inconsistent with the finding of similar craters in vitreous carbon prepared from specially purified materials (ash content ~ 5×10^{-6}%). Heat treatment in a stream of pure argon at 800–900° was found to lower the reactivity of the vitreous carbon samples. High-temperature treatment in argon is known [90] to lower the concentration of active centres, possibly by the removal of surface contaminants.

Lewis measured the activation energy for the oxidation of vitreous carbon and other graphitic materials at various temperatures by plotting the logarithm of the reaction rate against reciprocal absolute temperature (Arrhenius curves). The activation energy for the oxidation of vitreous carbon by dry air in the temperature range 600–800° was found to be approximately 43 kcal $mole^{-1}$. On adding 26 vol.% of water vapour to the air the activation energy fell to 31 kcal $mole^{-1}$, and the oxidation rate could either increase or decrease. The activation energy for the oxidation of graphite in moist air fell from 43 to 38 kcal $mole^{-1}$ in the same temperature range. On raising the temperature, the activation energy was found to increase. Among the explanations [90] which have been proposed are the influence of open pores, the accumulation of catalytically active contaminants at the surface of the vitreous carbon, and diffusion in the gas phase.

The oxidation of carbonaceous materials is accompanied by evolution of heat, which may result in an increase in the true reaction temperature. The magnitude of this effect increases with reaction rate. The variation of the rise in surface temperature of vitreous carbon and graphite samples with rate of oxidation [90] is illustrated in Fig. 18.

The rate of oxidation of vitreous carbon in argon containing carbon dioxide and water vapour varies linearly with temperature (900–1400°) and with the concentration of active impurities in the sample.

The mechanism of the oxidation of vitreous carbon has not been fully elucidated.

Grades of vitreous carbon prepared in the Soviet Union (by the present writers) have been found to be stable towards acids (HCl, HF, H_2SO_4), concentrated solutions of alkali (KOH), and bromine. However, our vitreous carbon, like other graphitic materials, is disintegrated (though to a lesser extent) by a mixture of concentrated H_2SO_4 + HNO_3 (1 : 1 by volume) and by chromic acid mixture (a 3% solution of $K_2Cr_2O_7$ in concentrated H_2SO_4).

Table 10. Oxidation resistance of graphitic materials.

Material	Time for specified weight loss (%), in min			
	70	80	90	100
Artificial graphite	68	95	110	140
Thermal graphite	120	138	175	230
High-density graphite	160	185	225	275
Vitreous carbon	205	225	270	365

The vitreous carbon prepared in the Soviet Union is also stable towards the following media: a) fused alkali metal chlorides (NaCl, KCl, etc.) saturated with hydrogen chloride, with pure hydrogen, and also at the interface between the melt and the gas phase at 800–1000°; b) a fused mixture of chlorides and fluorides of the alkali metals (NaCl, HCl, NaF) in the presence of argon and at temperatures in the range 800–1000°; c) a fused mixture of lithium and potassium chlorides in the presence of chlorine at 700°; d) a fused mixture of lithium and potassium chlorides containing uranium oxide chlorides; e) cryolite–alumina melts in an inert atmosphere at 960–1060°.

IV. APPLICATIONS OF VITREOUS CARBON

Vitreous carbon has an important future because of its unique properties (low permeability to liquids and gases, chemical inertness, high stability) and of its low electrical resistivity and high thermal stability in inert media.

Impervious carbon is an important material for the fabrication of cans for fuel elements in nuclear reactors [4,6,92].

The high chemical stability and low electrical resistance of vitreous carbon offer unique advantages in the preparation of electrodes for a variety of electrochemical purposes [93,94].

There are interesting prospects of applying vitreous carbon as a construction material for chemical plant designed to operate in aggressive media: reactive gases and liquids, fused metals and electrolytes, radioactive products [86].

The new material can be used to fabricate laboratory ware for the vacuum evaporation of metals (e.g. aluminium, gold), and for reactions in fused alkalies, in strong acids, or in fused metals (e.g. liquid bismuth) [5].

Apparatus made of vitreous carbon has many definite advantages over alternative materials (nickel, platinum, tantalum, glass, and silicon) for the zone refining of metals and for the preparation of specially pure compounds [76].

Corrosion-resistant coatings for a variety of articles can be made of vitreous carbon.

Because of its high purity, imperviousness to gases, non-wetting properties, and chemical inertness, vitreous carbon is ideally suitable for use as a "crucible" in semiconductor technology and in the optical industry (e.g. for the preparation of large single crystals of CaF_2 and MgF_2). [5]

The electrical resistivity of vitreous carbon is adequate for the fabrication of resistance heaters. Small-scale heater elements made of GC-30 vitreous carbon are becoming commercially available [25].

Vitreous carbon can withstand very high temperatures and is therefore used as a construction material for the production of silicon carbide and to handle liquid bismuth [2,5]. We may expect items currently made of high-purity molybdenum, quartz, pyrolytic graphite, fused alumina, etc. to be gradually replaced by vitreous carbon items [3].

Because of its high resistance to thermal shock, vitreous carbon can be used in high-temperature technology to fabricate sheaths for temperature measuring apparatus operating in aggressive media [2,5], and because of its high mechanical strength it can be used in abrasion-resistant articles such as dies [96] and components for handling piece-parts [3,5].

Addition of 0.5–1.0% of vitreous carbon to carbon powders for the production of electric carbon brushes has been found [97] to increase the service life of the product from 7300 to 11 500 h.

In addition to the above applications, vitreous carbon is beginning to find outlets in a great variety of industrial operations [25,54,76]. Surge arresters for the telephone network were tested under severe conditions and found to be very reliable. Vitreous carbon welding rods for spot-welding aluminium last longer than ordinary graphite rods. The material can be used for casting metallic articles in precision moulds, in the preparation of microphonic powders, and as a heat shield [76].

Thread guides of vitreous carbon, used in the yarn industry, overcome the problem of static electrification which arises when electrical insulators are used for the guides [76].

Vitreous carbon filaments may find applications in space exploration, in aviation, and in other fields of activity by virtue of their low specific gravity, high tensile strength, and high thermal stability.

Vitreous carbon made in the Soviet Union [18] have been very highly rated for use as electrodes in chloride and cryolite–alumina melts, and in mixtures of alkali metal chlorides and fluorides in an atmosphere of argon, hydrogen, chlorine, hydrogen chloride, and H_2 + HCl mixtures at temperatures up to 1000°. Vitreous carbon electrodes are indifferent to melts of lithium and potassium chlorides containing uranium oxide chlorides. Vitreous carbon electrodes are beginning to replace platinum electrodes.

The superiority of vitreous carbon over other graphitic materials is very evident even in containers for molten indium, which overcome the problem of metal "seepage" and give a purer product because they are free from open pores.

Vitreous carbon has been used in research on crystal growth by the electrolysis of molten salts.

Thermocouple pockets made of vitreous carbon have been thoroughly tested, with favourable results.

Because of the unique properties of vitreous carbon, a much longer service life can be confidently expected from articles and fixtures made of this material instead of ordinary graphite. The range of vitreous carbon articles which are becoming available, and the number of applications of the material, are continuously increasing.

REFERENCES

1. A. S. Fialkov, A. I. Baver, et al., Uspekhi Khim., **34**, 132 (1965) [Russ. Chem. Rev., No. 1 (1965)].
2. K. Yamada, Electronic Materials and Parts, **2**, 98 (1963).
3. S. Yamada, Kagaku to Kogyo, **16**, 52 (1963); VINITI Translation No. 38554/4.
4. S. Yamada, Nuclear Eng., **9**, 41 (1963).
5. B. Findeisen, Die Technik, **23**, 392 (1968).
6. B. P. 860 342/1961.
7. B. P. 860 340/1961; Chem. Abs., **56**, 3373d (1962).
8. US P. 3 104 159/1963; Chem. Zentr., **136**, I, 2108 (1965) [Chem. Abs., **60**, 1361g (1964)].
9. H. H. Losty and H. D. Blakelock, Society of Chemical Industry, Second Industrial Carbon and Graphite Conference, 7–9 April, London, 1965, 551.
10. H. W. Davidson, "Nuclear Graphite", Paris, OEEC, 1961, p. 209.
11. S. Otani, Kegyo Kagaku Zasshi, **62**, 871 (1959); Chem. Abs., **57**, 169225 B (1962).
12. B. P. 889 351/1958.
13. M. S. Dudkin, Uspekhi Khim., **31**, 1179 (1962) [Russ. Chem. Rev., No. 10 (1962)].
14. G. G. Dutton and A. M. Unrau, Canad. J. Chem., **40**, 2101 (1962).
15. H. W. Davidson, Nuclear Eng., **7**, 159 (1962).
16. S. Yamada and H. Sato, Nature, **193**, 261 (1962).
17. J. B. Donnet, Science et Enseignement scientifique, **6**, 33 (1965).
18. V. D. Chekanova, Symposium "Novoe v Elektrougol' nom Proizvodstve" (New Developments in Electrical Carbon Production), Informstandartelektro, Moscow, 1969, No. 3, p. 81.
19. Japan P. 24 580/1963.
20. B. P. 921 236/1963; Chem. Abs., **59**, 240a (1963).

21. Japan P. 569/1966.
22. Japan P. 5153/1964.
23. B. P. 968215/1959; Chem. Abs., 62, 256d (1965).
24. BRD P. 1213333/1966; Chem. Zentr., 138, I, 2131 (1967).
25. E. Saito and E. Yamada, Kogyo Zaire, 14, No. 12, 46 (1966).
26. US P. 3109712/1963; Chem. Zentr., 136, I, 2305 (1965).
27. B. M. Barykin, E. G. Spiridonov, and A. S. Tarabanov, Khim. Tverdogo Topliva, No. 2, 116 (1967).
28. Japan P. 21957/1963.
29. Japan P. 9554/1963.
30. Japan P. 11757/1964.
31. B. P. 956452/1964.
32. B. P. 1024971/1962.
33. French P. 1331683/1963.
34. Japan P. 6825/1964.
35. B. P. 946246/1964.
36. Japan P. 1527/1966.
37. K. Kawamura and G. M. Jenkins, J. Materials Sci., 5, 262 (1970).
38. Japan P. 489546/1967.
39. Japan P. 17655/1964.
40. S. Yamada and M. Yamamoto, Carbon, 6, 741 (1968).
41. A. S. Fialkov, V. D. Chekanova, P. A. Pshenichkin, V. S. Samoilov, and L. S. Tyan, Khim. Tverdogo Topliva, No. 3, 132 (1970).
42. V. D. Chekanova, A. S. Fialkov, I. M. Yurkovskii, P. M. Rybak, and B. I. Dyuzhikov, Khim. Tverdogo Topliva, No. 5, 103 (1970).
43. E. V. Orobchenko and N. Yu. Pryanishnikova, "Furanovye Smoly" (Furan Resins), Gostekhizdat, Kiev, 1963.
44. L. A. Igonin and K. I. Turchaninova, Dokl. Akad. Nauk SSSR, 150, 1280 (1963).
45. S. Mizushima and H. Kishigama, Symposium on Carbon, July 20–23 1964, Tokyo, 1964, Session 4, p. 158.
46. Yu. S. Lipatov, A. Ya. Tsybul'ko, and T. E. Lipatova, Vysokomol. Soed., 6, 1054 (1964).
47. A. S. Fialkov, V. D. Chekanova, V. S. Samoilov, T. I. Bertush, and E. S. Mikhailov, Khim. Tverdogo Topliva (in press).
48. K. Ouchi, Carbon, 4, 59 (1966).
49. L. I. Komarova, V. V. Korshak, V. A. Sergeev, L. V. Kozlov, and B. V. Lokshin, Zhur. Prikl. Spektrosk., 6, 501 (1967).
50. A. H. J. Gross, J. Appl. Chem., 7, 562 (1957).
51. V. V. Korshak, V. A. Sergeev, L. V. Kozlov, and L. I. Komarova, Plasticheskie Massy, No. 2, 33 (1966).
52. E. B. Trostyanskaya, E. S. Venkova, L. V. Aristovskaya, B. M. Kovarskaya, and G. L. Slonimskii, Plasticheskie Massy, No. 2, 61 (1968).
53. H. Honda, S. Tayda, S. Kanoka, and T. Furuto, Carbon, 3, 3 (1965).
54. "Marki Grafita Vypuskaemye za Rubezhom" (Grades of Imported Graphite), Nauch. Issled. Inst. Grafita, 1968, No. 2, p. 37.
55. M. J. Parisot, Rev. hautes Temperatures et Refractaires, 1, 171 (1964).
56. Production Eng., 36, 320 (1965).
57. M. Otterbein and L. Bonnetain, Carbon, 6, 877 (1968).
58. S. Yamada and H. Cato, Verres et Refractaires, 17, 102 (1963).
59. V. S. Chirkin, "Teplofizicheskie Svoistva Materialov Yadernoi Tekhniki" (Thermal Properties of Nuclear Materials), Atomizdat, Moscow, 1968.
60. T. Noda and M. Inagaki, Bull. Chem. Soc. Japan, 37, 1709 (1964).
61. W. V. Kotlensky and H. E. Martens, Nature, 205, 1246 (1965).
62. W. V. Kotlensky and H. E. Martens, see Ref. 45, Session 5, p. 191.
63. S. Nakamura, T. Ishii, and S. Yamada, see Ref. 45, Session 9, p. 354.
64. D. B. Fischbach, Nature, 217, 840 (1968).
65. D. B. Fischbach, Carbon, 5, 565 (1967).
66. S. Yamada, H. Cato, and T. Ischii, Carbon, 2, 253 (1964).
67. T. Yamaguchi, Carbon, 1, 535 (1964).
68. T. Yamaguchi, Carbon, 1, 47 (1963).
69. T. Tsuzuku and K. Saito, see Ref. 45, Session 4, p. 161.
70. T. Tsuzuku and K. Saito, Jap. J. Appl. Phys., 5, 738 (1966).
71. B. E. Warren and P. Bodenstein, Acta Cryst., 20, 602 (1966).
72. P. W. Selwood, "Magnetochemistry" (Translated into Russian), Inostr. Lit., 1958.
73. A. S. Fialkov, "Formirovanie Struktury i Svoistv Uglegrafitovykh Materialov" (Development of Structure and Properties in Graphitic Materials), Izd. Metallurgiya, Moscow, 1965.
74. S. E. Vyatkin, A. N. Deev, V. G. Nagornyi, V. S. Ostrovskii, A. M. Sigarev, and G. A. Sokker, "Yadernyi Grafit" (Nuclear Graphite), Atomizdat, Moscow, 1967.
75. V. I. Kasatochkin and G. B. Finkel'shtein, Dokl. Akad. Nauk SSSR, 149, 629 (1963).
76. New Scientist, 36, 761 (1967).
77. G. B. Skripchenko and V. I. Kasatochkin, Symposium "Strukturnaya Khimiya Ugleroda i Uglei" (Structural Chemistry of Carbon and Coal), Izd. Nauka, Moscow, 1969, p. 67.
78. T. Noda and M. Inagaki, Bull. Chem. Soc. Japan, 37, 1534 (1964).
79. K. Furukawa, Nippon Kessho Gakkaishi, 6, 101 (1964).
80. T. Noda and M. Inagaki, see Ref. 45, Session 3, p. 93.
81. S. Kakinoki, Acta Cryst., 18, 578 (1965).
82. T. Noda and H. Cato, Carbon, 3, 289 (1965).
83. T. Noda, Carbon, 6, 125 (1968).
84. W. C. Chard, R. D. Reiswig, L. S. Lewinson, and T. D. Baker, Carbon, 6, 950 (1968).
85. J. C. Lewis, B. Redfern, and F. C. Cowlard, Solid State Electronics, 6, 251 (1963).
86. Anon., Metallurgia, 67, 208 (1963).
87. J. Yamada, Eng. Materials, 11, 101 (1963).
88. M. K. Halpin and G. M. Jenkins, Proc. Roy. Soc., 313A, 421 (1969).
89. F. Pernot and C. Kojima, Verres et Refractaires, 20, 343 (1966).
90. J. C. Lewis, see Ref. 9, p. 282.
91. L. C. Blackman, Carbon, 5, 196 (1967).
92. French P. 1466386/1967.
93. H. E. Zittel and F. J. Miller, Analyt. Chem., 37, 200 (1965).
94. K. Swabe and H. J. Gens, Chem. Technik, 19, 309 (1967).
95. Tokai Technol. J., 22, 41 (1962).
96. French P. 1475809/1966.
97. B. P. 1058683/1967.